Electronic Supplementary Material (ESI) for ChemComm.

Supporting Information: Ultrathin zigzag-surface copper nanowires assembled hierarchical microspheres to enhance oxygen reduction catalysis

Zhu Yan, Zhang Xue-Ying, Zhang Yong*, Zhou Guan-Yu, Zhao Hong*

Department of Materials Science and Engineering, Dalian Jiaotong University, Dalian 116028, China;

*Corresponding author: zhaohong@djtu.edu.cn (Zhao Hong)
*Corresponding author: zhangyong@126.com (Zhang Yong)

Experimental Procedure and Calculation Methods

a) Low temperature growth of Cu-based catalysts

Low temperature growth of Cu-based catalysts was conducted in 0.1mol/L $CuSO_4$ solution at 273 K temperature under DC power electric field. The positive and negative poles of DC power electric field were connected to copper foil and Cu-Zn-Al plate, respectively. Under 273 K temperature, the low temperature growth of Cu-based catalysts was carried out at 1V, 5V, 9V and 13V voltages, respectively. In order to guarantee even distribution of electric field in $CuSO_4$ solution and drive directional diffusion of copper ions from cathode to anode, the cathode copper foil should face the anode steel plate, and the anode area is larger than the cathode area. The distance between cathode copper foil and anode steel plate is 10-12 mm.

b) Microstructure characterization

The morphology of Cu-based catalysts was observed using scanning electron microscopy (SEM, SUPRA-55, Germany) and transmission electron microscopy (HRTEM, JEOL2100F, Japan). The crystallographic characterization was performed by an X-ray diffraction (XRD, Empyrean, Holland) with Cu K_α radiation at a scanning speed of 6 °/min. The compositions of Cu-based catalysts were analyzed using an X-ray photoelectron spectroscope (XPS Thermo Scientific K-Alpha, US) at room temperature.

The optical contact angle meter system (JC2000D1, China) was used to measure the contact angle of lotus leaf and Cu-based catalysts, respectively. The underwater contact angles of water or oil droplets on the surface of lotus leaf and Cu-based catalysts were measured by a contact-angle system (HARKE, China), which could calculate contact angles from the drop shapes with an accuracy of ±0.1°. In order to reduce testing error, each sample was measured for five times and an average value of five contact angles was employed [1].

c) Electrochemical characterization

All the electrochemical tests were carried out in an electrochemical workstation (PGSTAT302 N, Ecochemie Co. Holland) under room temperature (303 K) and low temperature (273 K), respectively. These electrochemical measurements were performed in a traditional three-electrode cell system with the platinum mesh electrode and saturated calomel electrode (SCE) as the counter electrode and the reference electrode, respectively. Moreover, a rotating disk electrode was deposited with catalysts as the working electrode, in which the catalyst ink was made by mixing 3.0 mg Cu-based catalyst and 25μL 5wt% Nafion solution.

The ORR activities of the catalysts were evaluated by cyclic voltammetry (CV) and linear sweep voltammetry (LSV) tests in nitrogen and oxygen saturated 0.1 mol L^{-1} KOH solution successively at a scan rate of 50 mV s^{-1}. Subsequently, the LSV curves of the catalysts were measured in oxygen saturated 0.1 mol L^{-1} KOH solution with a rotating speed of 500 rpm. As a benchmark, the ORR activity of commercial Pt/C (20 wt% Pt on carbon black, HiSPEC 3000, Johnson Matthey) working electrode was also tested, in which the loading of Pt/C (20%) on the surface of the electrode is 0.2 mg/cm^2.

In addition, the electron transfer numbers were calculated using the Koutecky-Levich equation [2]:

$$1/j = 1/j_L + 1/j_K = 1/(B\omega^{1/2}) + 1/j_K \quad (1)$$

$$B = 0.62nFC_0(D_0)^{2/3}\, v^{-1/6} \quad (2)$$

$$j_K = nFKC_0 \quad (3)$$

Where, j is the measured current density; j_L and jK are the diffusion- limiting and kinetic current densities, respectively; n represents the overall number of electrons gained per O_2; F is the Faraday constant (F = 96485 C mol^{-1}); C_0 is the bulk concentration of O_2; D_0 is the diffusion coefficient of O_2 in 0.1 M KOH electrolyte; v is the kinetic viscosity of the electrolyte; ω is the angular velocity of the disk (ω = 2πN, N is the linear rotation speed) and k is the electron transfer rate constant.

Moreover, rotating ring-disk electrode (RRDE) tests were performed to measure the H_2O_2 yields and electron transfer of all Cu-based catalysts. [3] For comparison, a 20wt% Pt/C sample was adopted in our experiment. The equations used to calculate n (the apparent number of electrons transferred during ORR) and H_2O_2 yields (the percentage of H_2O_2 released during ORR) are the following:

$$n = 4\, I_D/(I_D + I_R\, /N) \quad (4)$$

$$H_2O_2 \text{ yield} = 100 * (2 I_R /N)/(I_D + I_R /N) \quad (5)$$

Where I_R and I_D are the currents at ring and disk, respectively. N is the RRDE collection efficiency, which is calculated to 0.37 in our experiment.

Furthermore, the AC electrochemical impedance spectra (EIS) of Cu-based catalysts were measured in the frequency range from 1000000 Hz to 1 Hz. In order to realize an equilibrium state, all three-electrode cells for EIS tests were stabilized for twenty minutes before measurement.

d) Theoretical calculations.

The ORR activities of Cu-based catalysts were predicted by first-principles calculations using the Vienna ab initio simulation package (VASP) code within the framework of density functional theory (DFT). The triclinic Cn_3Zn crystallizes in the space group P1, in which the lattice parameters of triclinic Cn3Zn are a=0.84 nm, b=0.45 nm, c=0.10 nm. The monoclinic CuO crystallizes in the space group 15 C2/C, and the lattice parameters of monoclinic CuO is a=0.46 nm, b=0.34 nm, c=0.51 nm. The cubic Cu_2O crystallizes in the space group 224 PN-3M, and the lattice parameters of cubic Cu_2O is a=b=c=0.42 nm. The exchange coorelation energy of electrons was described within the generalized gradient approximation (GGA) as parameterized by Perdew, Burke, and Ernzerhof.[4] The energy cut-off is set up to 300 eV, and the k-point sampling of the first Brillouin zone is set up to 6 × 6 × 6.

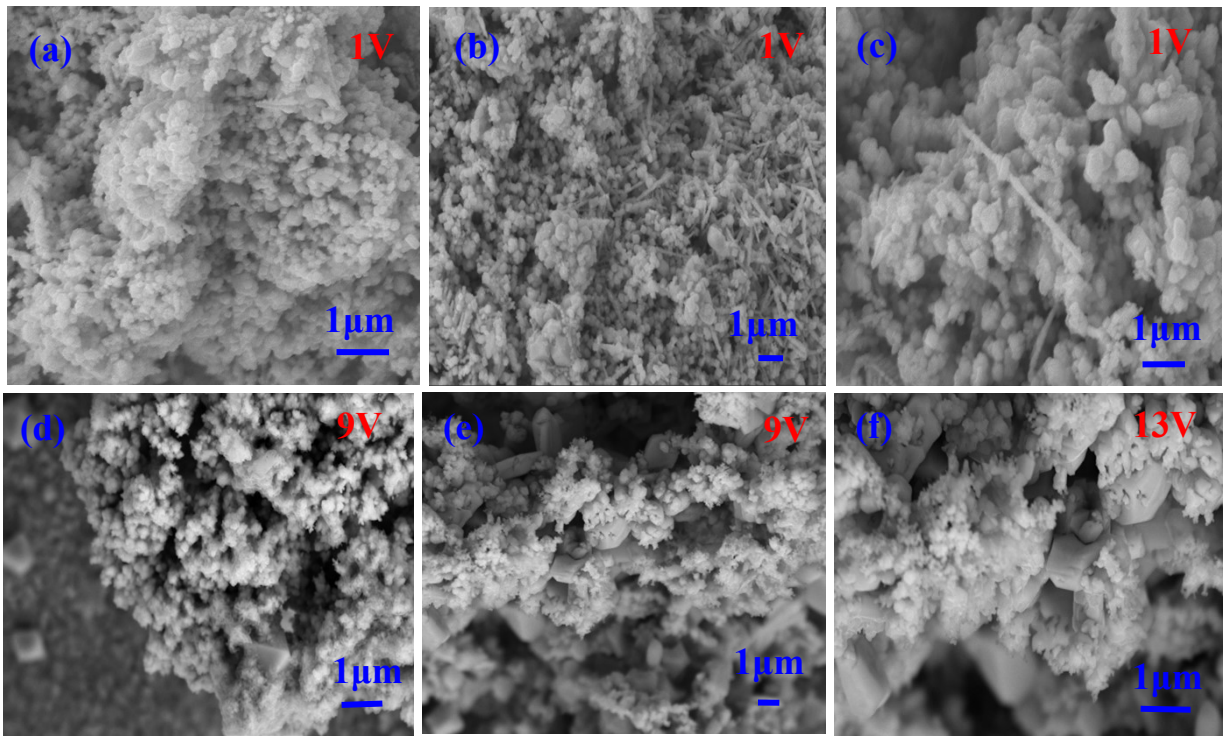

Fig. S1 SEM observation of Cu-based catalysts synthesized at different voltages

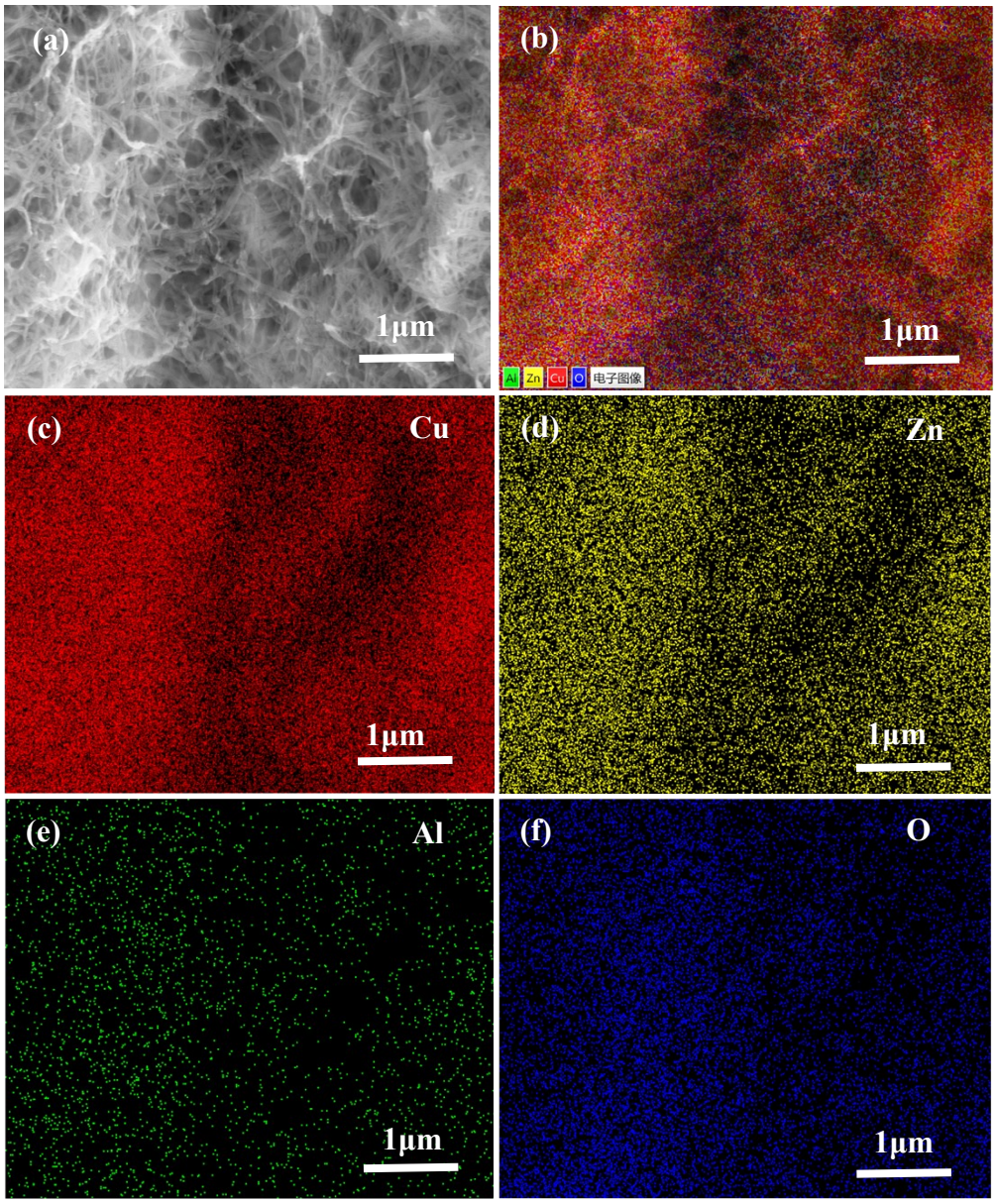

Fig. S2 EDS elemental analysis of ultrathin copper nanowires.

Fig. S3 is the XRD analysis of Cu-based catalysts obtained at different reaction voltages. The diffraction peaks at 49.6°and 87.5°are attributed to Cu_3Zn(200) and Cu_3Zn(110), respectively (JCPDS card, No. 03-065-6567). The diffraction peak at 42.6°is related to Cu_2O(200) and CuO(200) (JCPDS card, No. 00-034-1354, 01-078-0428). The diffraction peaks of Cu_2O(111) and Cu_2O(311) at 36.5°and 73.6°are also found (JCPDS card, No. 01-078-2072). Therefore, Cu_3Zn and Cu_2O are the main components of 5V voltage synthesized ultrathin copper nanowires.

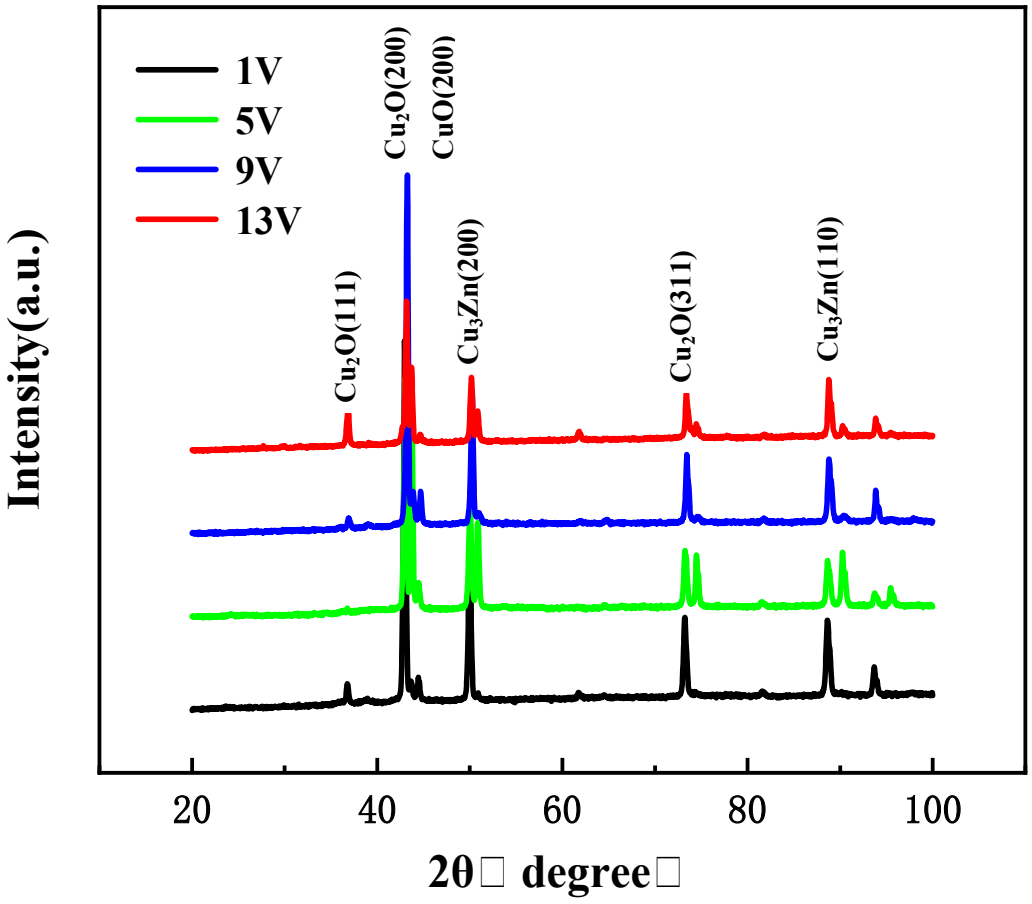

Fig. S3 XRD patterns of Cu-based catalysts synthesized at different voltages

To uncover the chemical states and chemical elemental compositions of ultrathin copper nanowires, XPS characterization is performed. As shown in Fig. S4, the characteristic weak satellite peaks of Cu^{+} 2p and Cu^{2+} 2p appeared at 947.0 eV and 943 eV binding energies, which suggests the existence of Cu_2O and CuO, respectively.[5, 6] Notably, $2p_{3/2}$ and $2p_{1/2}$ doublet peaks of Cu^{+} are revealed at 932.62 and 952.5 eV, respectively, [5, 6] as shown in Fig. S4(a). Obviously, Cu^{+} is present on the surface of ultrathin copper nanowires, which is in agreement with the above XRD analysis of Cu_2O phase. In the high-resolution O 1s XPS spectrum of Fig. S4(b), the deconvoluted two peaks at 531.2 eV and 532.2 eV are originated from surface adsorbed oxygen and adsorbed water molecules, respectively, suggesting the existence of O^{2-}. [7, 8]

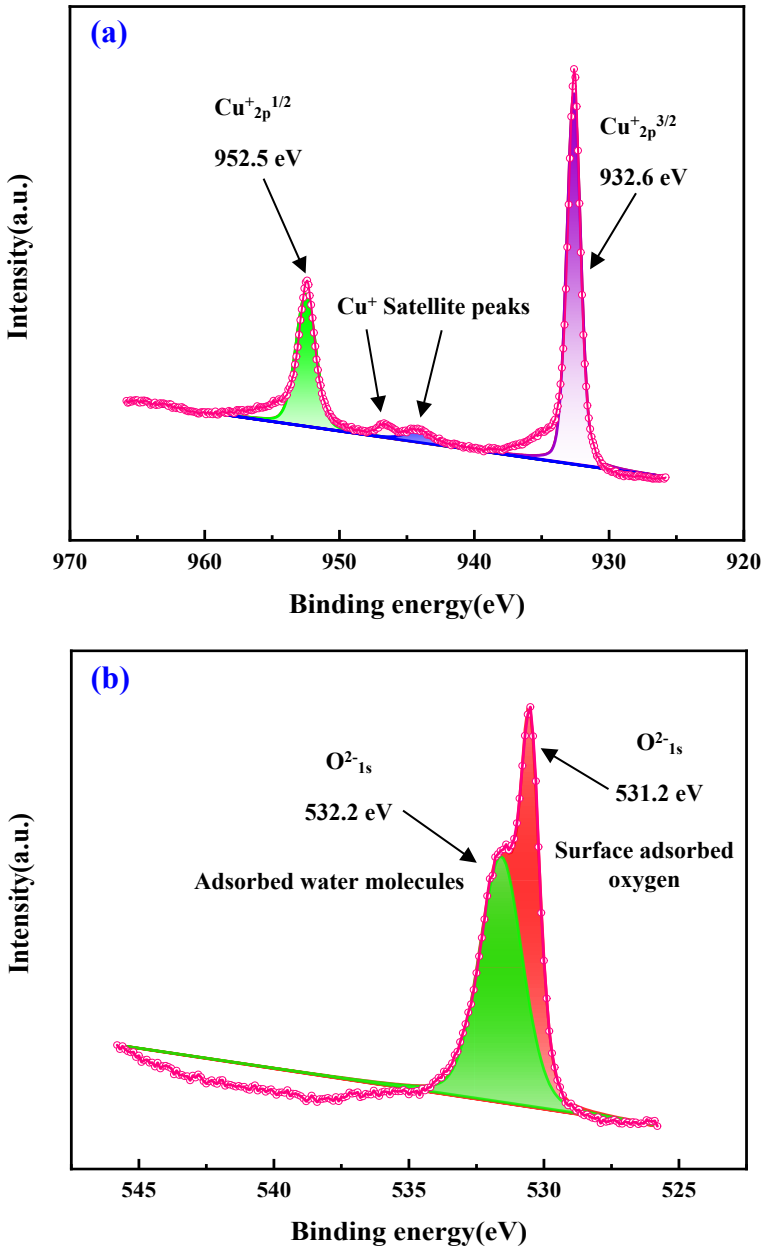

Fig. S4 XPS analysis of ultrathin copper nanowires

Under room temperature (303 K) and low temperature (273 K) tests the CV curves of ultrathin copper nanowires demonstrate obvious reduction peaks in oxygen saturated 0.1 mol L^{-1} KOH solution, indicating their ORR activities (Fig. S5, Fig. S6, Table S1 and Tables S2). Compared with other Cu-based catalysts, the ultrathin copper nanowires have much larger electrochemical surface-active area than other Cu-based catalysts, signaling their superior electrochemical properties. Under room temperature the onset potential and halfwave potential of ultrathin copper nanowires are 0.85 V and 0.78 V, respectively. In recent literatures Cu-based catalysts exhibit good ORR performances. For example, Yang et al reported a halfwave potential of 0.88 V for single atom copper catalyst in alkaline solution [9], and a halfwave potential of 0.89 V for single-site copper catalyst in alkaline media is reported by Sun et al [10]. Moreover, a halfwave potential of 0.83 V was reported in our recent experiment of Cu-O-C catalysts [7]. These ORR performances are much higher than those of Co_3O_4 nanosheets (0.8 V) [11] and NiO/CoO nanostructures (0.66 V) [12] cases, demonstrating the superior ORR performances of Cu-based catalysts.

Due to the high energy conversion efficiency, low emission pollution and quiet operation advantages, fuel cells can be viewed as the ideal new energy powers. Nevertheless, the slow kinetics of oxygen reduction reaction (ORR) of fuel cells limits their widely commercial applications. Nowadays, the exploration footsteps of human beings are reaching deep-sea, outer space and other extremely cold regions, and the slow ORR kinetics issue of fuel cells is especially obvious under these low temperature conditions. Compared to room temperature ORR activities, the low temperature ORR activities are much more difficult. Although Pt and Ir demonstrate good low temperature ORR activities, their high-cost disadvantages are still not satisfied. The good low temperature ORR activities of ultrathin copper nanowires will provide some insights for the low temperature commercial applications of fuel cells.

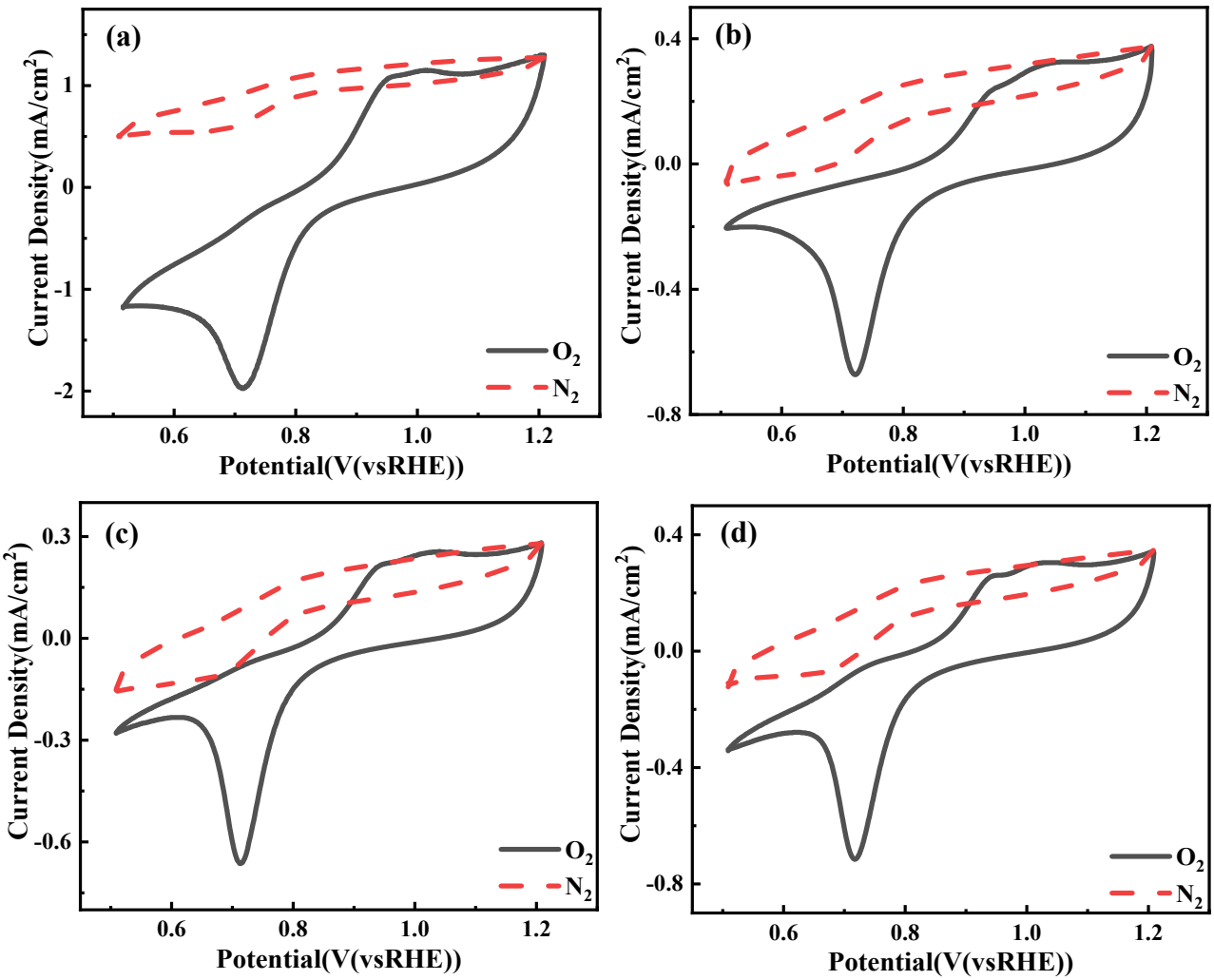

Fig. S5 Room temperature CV curves of Cu-based catalysts in nitrogen or oxygen saturated 0.1 mol L-1 KOH solution.

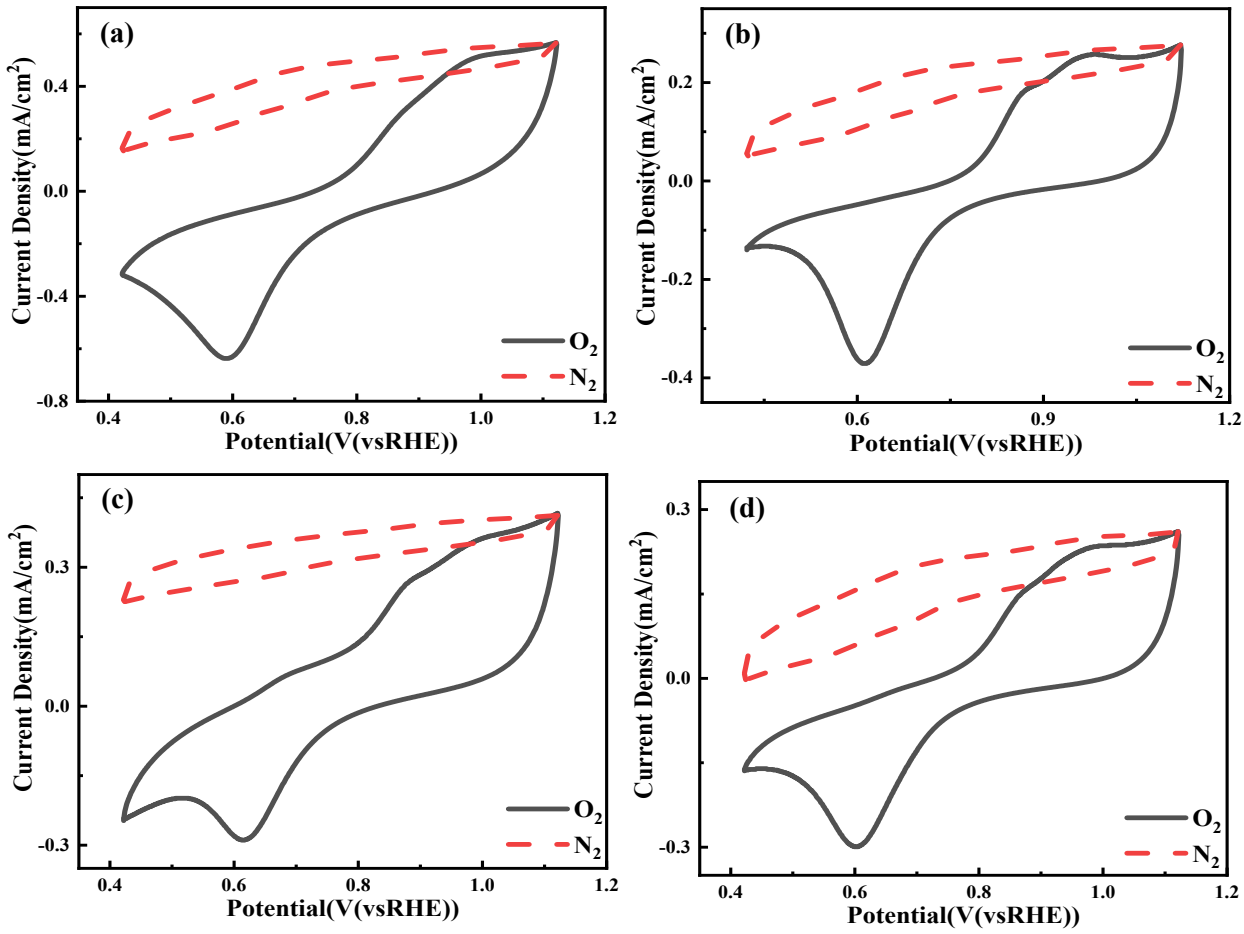

Fig. S6 Low temperature CV curves of Cu-based catalysts in nitrogen or oxygen saturated 0.1 mol L^{-1} KOH solution

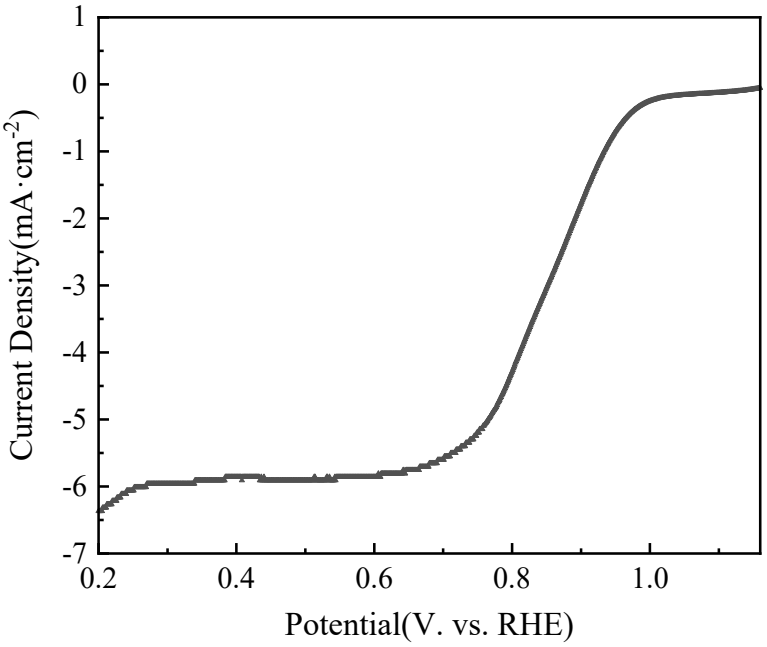

Fig. S7 LSV curve of 20wt% Pt/C catalyst

Table S1 Room temperature (303 K) onset potentials (E_{onset}) and halfwave potentials ($E_{1/2}$) of Cu-based catalysts synthesized at different voltages

Voltage (V)	1	5	9	13
Onset potential (V)	0.79	0.85	0.82	0.82
Halfwave potential (V)	0.76	0.78	0.73	0.75

Table S2 Low temperature (273 K) onset potentials (E_{onset}) and halfwave potentials ($E_{1/2}$) of Cu-based catalysts synthesized at different voltages

Voltage (V)	1	5	9	13
Onset potential (V)	0.77	0.82	0.79	0.8
Halfwave potential (V)	0.71	0.73	0.72	0.71

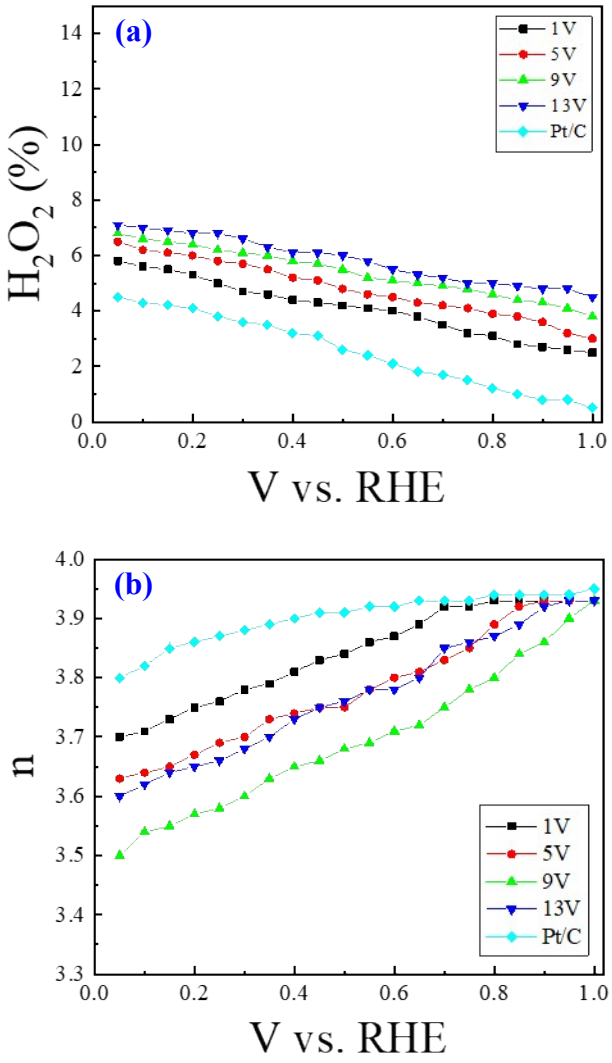

Fig. S8 The H_2O_2 yields (a) and electron transfer (b) of Cu-based catalysts and 20wt% Pt/C sample

ORR occurs at the triple phase regions of electrocatalysts, in which O_2 diffusion and charge transfer are two critical steps to govern the kinetics of oxygen reduction catalysis. It is well known that EIS is a powerful technique to investigate the mass diffusion and charge transfer phenomena of fuel cells, lithium batteries and other new energy conversion systems. To elucidate the ORR kinetics of ultrathin copper nanowires, EIS measurements of ultrathin copper nanowires are conducted (Fig. S9(a-b)).

It is reported that the Randles circuit is usually adopted to describe the oxygen reduction reaction (ORR) kinetics for fuel cells, in which the O_2 diffusion coefficients of ORR are closely related to the Warburg impedance Z_W, charge transfer resistance R_{ct} and double-layer capacity C_{dl} of the equivalent electrical circuits (EECs) in EIS results [13, 14]. As shown in Table S3 and Table S4, the Cu-based catalyst synthesized at 5 V demonstrates the fastest electron transport in all Cu-based catalysts with the lowest interface charge transfer resistance (R_{ct}).

Calculating the diffusion length δ^2 and diffusion time τ_D from the Randles circuit of EIS results, the O_2 diffusion coefficients D_{eff} can be given by equation:

$$D_{eff} = \delta^2/\tau_D \quad (6)$$

It turns out that the O_2 diffusion coefficient of 5 V voltage synthesized ultrathin copper nanowire sample is obviously higher than those of other Cu-based catalysts, as shown in Fig. S9. These results confirm the good O_2 diffusion abilities promoted by zigzag-surface copper nanowires. In addition, i-t tests of Cu-based catalysts are performed under room temperature (303 K) and low temperature (273 K), respectively, which reveal that the current density of ultrathin copper nanowires is higher than other Cu-based catalysts (Fig. S9(c-d)), demonstrating good electrochemical durability in 0.1 mol L^{-1} KOH solution.

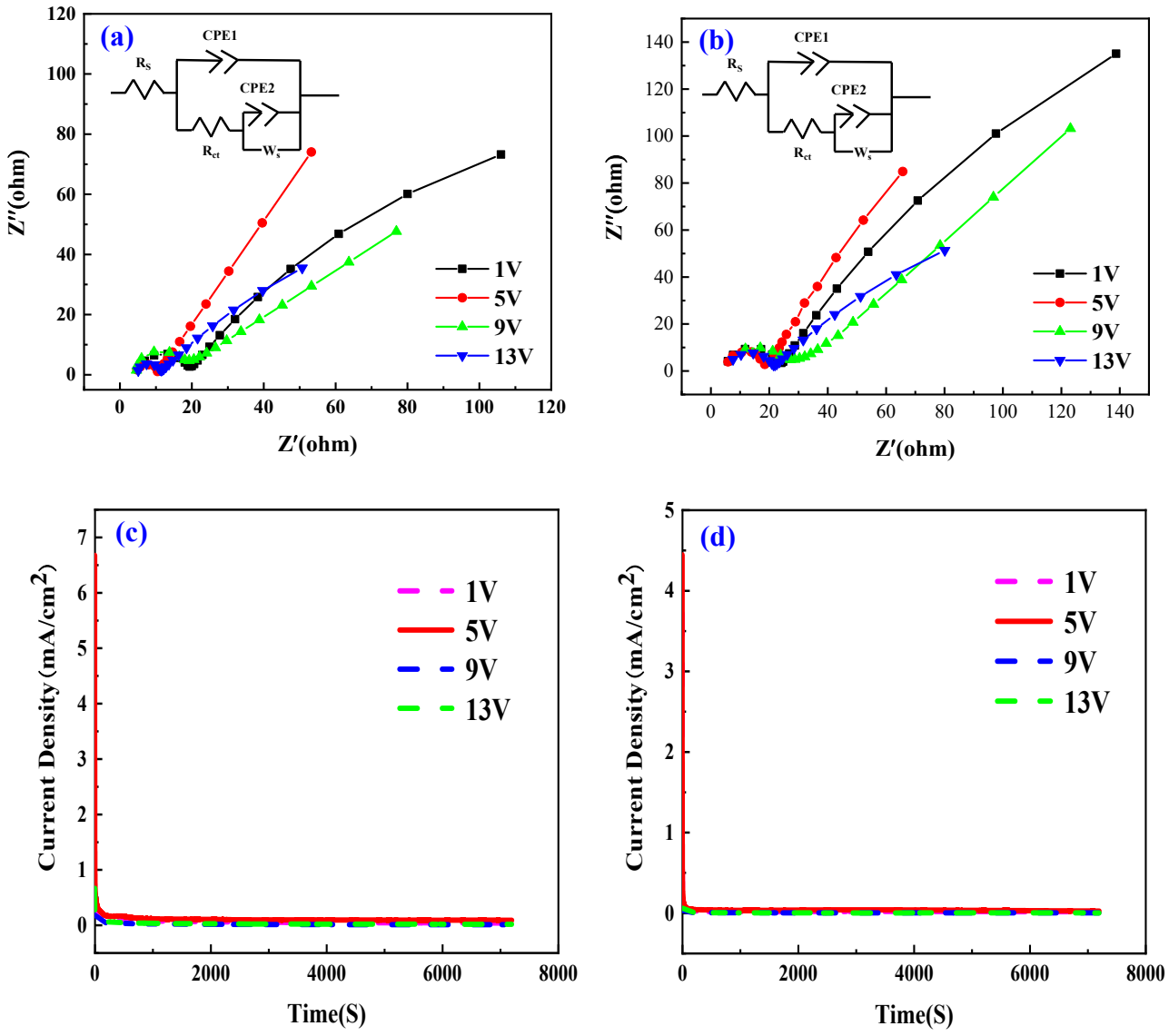

Fig. S9 Nyquist diagram and i-t tests of Cu-Zn-Al catalysts in oxygen saturated 0.1 mol L^{-1} KOH solution
(a) Room temperature Nyquist diagram; (b) Low temperature Nyquist diagram
(c) Room temperature i-t tests; (d) Low temperature i-t tests
Where, the insets of (a) and (b) are their equivalent circuits, respectively

Table S3 Room temperature (303 K) charge transfer resistance (R_{ct}) and diffusion resistance (R_d) of Cu-based catalysts synthesized at different voltages

Voltage (V)	1	5	9	13
R_{ct} (Ω cm^2)	0.21	0.18	0.23	0.28
R_s (Ω cm^2)	0.35	0.32	0.38	0.45

Table S4 Low temperature (273 K) charge transfer resistance (R_{ct}) and diffusion resistance (R_d) of Cu-based catalysts synthesized at different voltages

Voltage (V)	1	5	9	13
R_{ct} (Ω cm^2)	0.32	0.26	0.33	0.40
R_s (Ω cm^2)	0.44	0.41	0.50	0.51

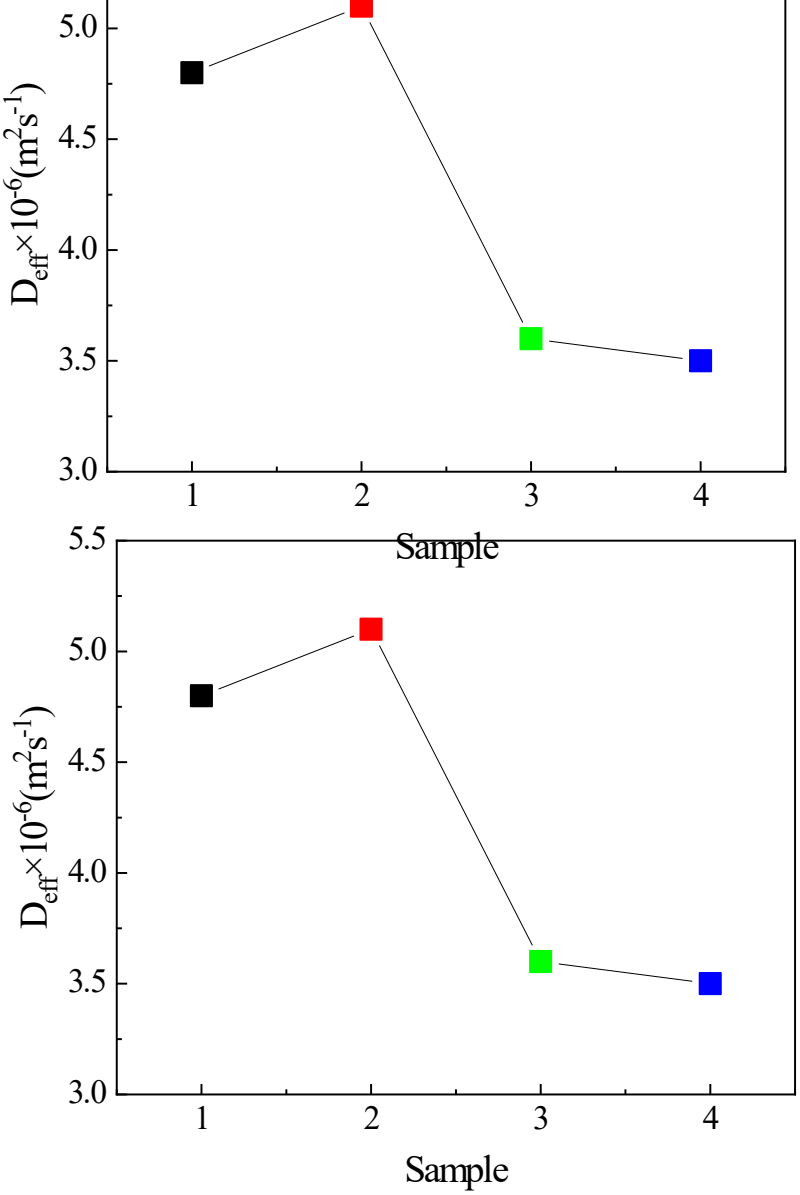

Fig. S10 O_2 diffusion coefficients of Cu-based catalysts synthesized at different voltages

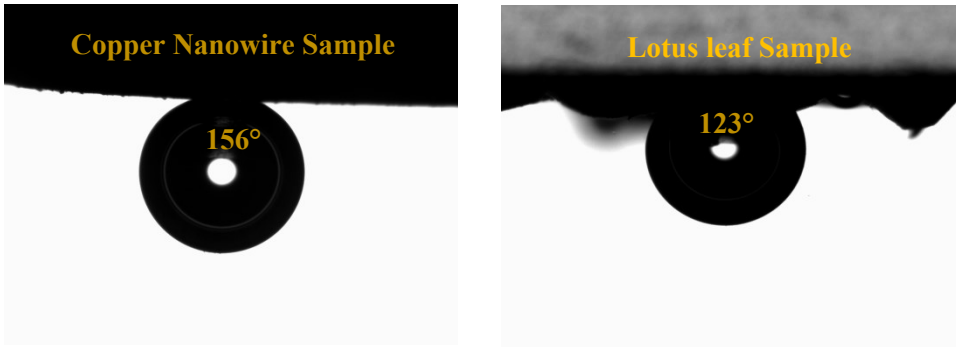

Fig. S11 Underwater air-bubble contact-angle tests of copper nanowires and lotus leaf samples

Notes and references

1 K Yin, YX Song, XR Dong, C Wang, JA Duan, Underwater superoleophobicity, anti-oil and ultra-broadband enhanced absorption of metallic surfaces produced by a femtosecond laser inspired by fish and chameleons. Sci. Rep. 2016, 6: 36557.
2 LT Cui, LR Cui, ZJ Li, J Zhang, HM Wang, SF Lu, Y Xiang, A copper single-atom catalyst towards efficient and durable oxygen reduction for fuel cells. J. Mater. Chem. A 2019, 7: 16690-16695.
3 GX Zhang, Q Wei, XH Yang, AC Tavares, SH Sun, RRDE experiments on noble-metal and noble-metal-free catalysts: Impact of loading on the activity and selectivity of oxygen reduction reaction in alkaline solution. Appl. Catal. B: Environ 2017, 206: 115-126.
4 JP Perdew, K Burke, M Ernzerhof, Generalized gradient approximation made simple. Phys. Rev. Lett. 1996, 77: 3865.
5 LY Li, RM Chen, JL Wang, KW Wang, Y Zhou, MY Xing, F Dong, Dynamic in-situ formation of Cu_2O sub-nanoclusters through photoinduced pseudo-Fehling's reaction for selective and efficient nitrate-to-ammonia photosynthesis. Angew. Chem. Int. Ed. 2024, 63: e202317575.
6 Y Xiong, SB Wang, WX Chen, J Zhang, QH Li, HS Hu, LR Zheng, WS Yan, L Gu, DS Wang, YD Li, Construction of dual-active-site copper catalyst containing both Cu-N_3 and Cu-N_4 Sites. Small 2021, 17: 2006834.
7 H Idriss, On the wrong assignment of the XPS O1s signal at 531–532 eV attributed to oxygen vacancies in photo- and electro-catalysts for water splitting and other materials applications. Surf. Sci. 2021, 712: 121894.
8 TJ Frankcombe, Y Liu, Interpretation of Oxygen 1s X‑ray Photoelectron Spectroscopy of ZnO. Chem. Mater. 2023, 35: 5468-5474.
9 ZH Yang, KY Jiang, GS Tong, CC Ke, HF Wu, P Liu, JC Zhang, HP Ji, JH Zhu, CB Lu, XD Zhuang, Copper-involved highly efficient oxygen reduction reaction in both alkaline and acidic media. Chem. Eng. J. 2022, 437: 135377.
10 TT Sun, YL Li, TT Cui, LB Xu, YG Wang, WX Chen, PP Zhang, TY Zheng, XZ Fu, SL Zhang, ZD Zhang, DS Wang, YD Li, Engineering of coordination environment and multiscale structure in single-site copper catalyst for superior electrocatalytic oxygen reduction. Nano Lett. 2020, 20: 6206-6214.
11 RK Bera, HJ Park, R Ryoo, Co_3O_4 nanosheet on zeolite-templated carbon as an efficient oxygen electrocatalyst for zinc-air battery. J. Mater. Chem. A 2019, 7: 9988-9996.
12 DD Yu, Y Zhang, HQ Yu, H Zhao, Low temperature synthesis of NiO/CoO nanostructures to enhance their low temperature oxygen reduction catalysis. Micron 2022, 161: 103326.
13 W Aït-Idir, PZ Wu, R Sgarbi, Q Labarde, S Touhami, M Daoudi, AE kaddouri, JC Perrin, J Dillet, C Marty, F Micoud, M Chatenet, O Lottin, J Mainka, Oxygen diffusion impedance in proton exchange membrane fuel cells-insights into electrochemical impedance spectra and equivalent electrical circuit modeling. Electrochim. Acta 2023 472: 143430.
14 TQ Nguyen, C Breitkopf, Determination of diffusion coefficients using impedance spectroscopy Data. J. Electrochem. Soc. 2018, 165: E826-E831.